Experimental Thermal and Fluid Science 55 (2014) 221–227

Contents lists available at ScienceDirect

Experimental Thermal and Fluid Science

journal homepage: www.elsevier.com/locate/etfs

The acoustic signature of gas bubbles generated in a liquid cross-flow

R. Chicharro *, A. Vazquez

Universidad Nacional Autónoma de México – Facultad de Ciencias, Laboratorio de Fluidos, Av. Universidad 3000, Delegación Coyoacán, C.P. 04510 México, D.F., Mexico

ARTICLE INFO

Article history:
Received 4 June 2013
Received in revised form 1 March 2014
Accepted 15 March 2014
Available online 1 April 2014

Keywords:
Bubble growth
Capillary waves
Liquid cross-flow
Minnaert-frequency
Passive acoustic
Neck collapse

ABSTRACT

Observations of air bubble growth in a quiescent liquid and in a liquid cross-flow by means of a high-speed camera and piezoelectric-hydrophone in a synchronous experimental setup are performed. Using the passive acoustical method, one observes a beat-wave phenomenon when the feed magnitude of liquid cross-flow is increased from 43 to 128 mm/s and this is corroborated by the appearance of peaks in spectral and spectrogram analyses respectively. A fit to experimental data by a theoretical-model indicates that the beat-signal is the result of under and overdamped systems. The bubble video-images show the asymmetric travel of bubble-surface ripples after the neck collapse. The acoustic comparison exhibits a beat signal as a result of capillary – wave superposition, which is in agreement with earlier results on bubble fragmentation in a locally sheared flow.

1. Introduction

Bubbly or dispersed-phase flows are of great interest in chemical and pharmaceutical industries, and recently have received a special focus in the environmental and marine sciences, where the issue is related to global warming through the release of methane bubbles from the sea to the atmosphere. The form in which the bubbles are generated plays an important role in the energy and mass transport efficiency. They are commonly formed using capillary tubes, perforated plates, ceramic stones, sieve arrays, etc. Bubble formation from a submerged orifice in quiescent water (in which liquid cross-flow is absent) has attracted the attention of many studies over the years [1–6]. Such studies have had good success in describing the formation size and rate as a function of the orifice geometry and feed rate. In contrast, bubble formation in industrial processes and nature often occurs for liquid cross-flows. For example currents are ubiquitous at sea, in rivers, and even in many lakes [7,8]. In industrial settings, circulations in bubble columns or flow across a sieve tray in distillation/absorption create liquid cross-flows [9,10]. The role of liquid cross-flows in bubble formation has been studied by some authors [11–15] with the consensus that the liquid cross-flow enhances bubble generation via easier and earlier detachment, leading to smaller bubble formation. The drag from the cross flow results in earlier bubble detachment, reducing the bubble diameter, increasing interfacial area generation, and thereby improving mass exchange [16]. In addition, bubble formation under a liquid cross-flow also sweeps the bubbles away from the region near the orifice, reducing the likelihood of coalescence. Due to the relationship between bubble size and cross flow, manipulating the cross flow can improve control over the bubble size and frequency [4]. Finally, liquid cross-flow induced bubble size distributions can impact significantly the bubble emission size distribution, and thus, the fate of seabed gases.

Video-image analysis is the most common bubble observation approach, allowing the measurement of flux, bubble size, and fluid motions [17–20]. Optical methods have been developed for in situ bubble detection using imaging systems, and generally use backlighting illumination. Another recently proposed approach for laboratory, field and industrial measurements is passive acoustics [21–23] which uses the sound produced by the bubble formation to derive the bubble size. This sound is a pulse that originates when bubble inflation leads to appearance of a neck (that connects the bubble's body to the orifice) that then collapses. Collapse of the air neck drives a bubble breathing mode which causes bubble volume oscillations within a narrow-frequency range band and an exponentially lightly-damped sinusoidal signal. The formation of this sound is characterized by the Minnaert frequency [24] and is given by,

$$f_o = \frac{1}{R_o}\sqrt{\left(\frac{3\gamma P_A}{4\pi^2\rho}\right)} \tag{1}$$

where f_0 is the frequency (Hz), R_0 is the equivalent bubble radius (the radius assuming the bubble is a spherical volume), P_A is the absolute liquid pressure (1×10^5 Pa), ρ is the liquid density

* Corresponding author. Tel.: +52 55 5622 4934.
E-mail address: rocio.chicharro@ciencias.unam.mx (R. Chicharro).

http://dx.doi.org/10.1016/j.expthermflusci.2014.03.011
0894-1777/

Nomenclature

A	amplitude, normalized	γ	specific heats ratio, dimensionless
f_0	frequency, Hz	δ	damping factor
P_A	liquid pressure, Pa	v	cross flow velocity, mms^{-1}
Re	Reynolds number, dimensionless	φ	phase factor
R_0	equivalent bubble radius, mm	ρ	liquid density, kg/m^3
t	time, s	μ	liquid viscosity, kg m^{-1} s^{-1}

(kg/m^3), γ is the ratio of specific heats for the gas assuming adiabatic compression and expansion, and (1) is valid for millimeter-scale bubbles. This Passive Acoustical Technique (PAT) and has been applied for bubble-size measurements in shallow waters [25] and in recent years the PAT also is used for the detection of bubble acoustical signals in a fluid cross-flow [26,27], anisotropy in the sound field originated by a bubble chain [28–30], sound generation on bubble coalescence following detachment [31], acoustical studies of injected bubbles [32] and eigenmodes of a pair or small group of bubbles [33].

The Minnaert relationship has been derived for radially symmetric bubbles in quiescent water. Thus, the appropriateness of its application to asymmetric bubble formation, such as for a liquid cross-flow, may be unclear, but critical for the correct measurement of the bubble size observations in a wide number of real world applications. In this study we observe the acoustical signals for air bubble growth and separation from a glass capillary tube in a laminar liquid cross-flow at different feed rates. The signals are analyzed to detect the breathing mode oscillations, and then are compared with air bubble data for formation in quiescent liquid (no cross-flow).

Although there is an extensive literature on the sound produced from bubble formation in quiescent liquid, studies on the sound generation, when the bubble neck breaks during bubble formation in a liquid cross-flow are not commonly found.

2. Experimental setup

The experimental set up is shown schematically in Fig. 1. Air is injected by a standard aquarium-pump (Elite 802 to 3.5 W, Canada) into a pre-saturation chamber, which prevents rapid changes in bubble volume after separation due to water vapor [34]. Gas then flows through coarse and fine bronze valves that control the flow rate into a cylindrical pressure chamber (5×10^{-6} m^3). The pressure chamber is connected to a glass capillary tube (Drummond Scientific, Broomall, PA, US), with an inner diameter of $990 \pm 10 \times 10^{-6}$ m, mounted on a twine plastic base. The capillary tube is centered in a glass (5×10^{-4} m wall thickness) water tank of $0.6 \times 0.3 \times 0.2$ m, which is filled with fresh water. The tank was designed to be large enough to reduce acoustic reverberation for millimeter-sized bubbles with walls, i.e., more than 20 bubble diameters. [35]. A submersible water-pump (Resun SP-1100 to 8 W) creates a uniform cross-flow in the tank in an isolated zone by feeding an L-shaped acrylic square tube. The bubbly flow is in the solitary range and in the constant volume range as indicated by the capacitance number (N_C) given by $N_C = V_{CH} g \rho_L / \pi (r_{cap}^2) P_{OR}$, where r_{cap} is the capillary internal radius, P_{OR} is the orifice pressure and V_{CH} is the volume chamber [36]. For our set-up, $N_C = 0.15$, which is within the range for steady flow and formation of solitary bubbles with the same volume ($N_C < 1$).

For each experiment, the airflow and currents were first allowed to stabilize for at least 10 min. Typical bubble formation rates were 0.33 Hz (a spacing 3 bubbles per second) over a time of 5 min, which give a set of 99 individual air bubbles. As a result, the measured values of equivalent spherical radius agreed to better than 2–3% (standard deviation) between bubbles and all values in this study are data set averages, while cross-flows ranged between 0 and 76 cm^3 s^{-1}. A laminar nozzle, consisting of a bundle of 25 plastic-tube orifices, each 10 cm long, and closed with two circular micro-fibers (cleaning-sponges) ensured a laminar fluid flow. The fluid profile was confirmed by qualitative observations of an organic-dye tracer (iodine) introduced into the L-shaped square tube. Bubbles were imaged with a digital high speed color camera (Olympus i-SPEED, Olympus KeyMed, Ltd., United Kingdom) at 1000 frames s^{-1} with a resolution of 800×600 pixels by 12 bits. A 1000-watt halogen lamp illuminated a diffusion screen to provide back illumination with minimal small scale in-homogeneity.

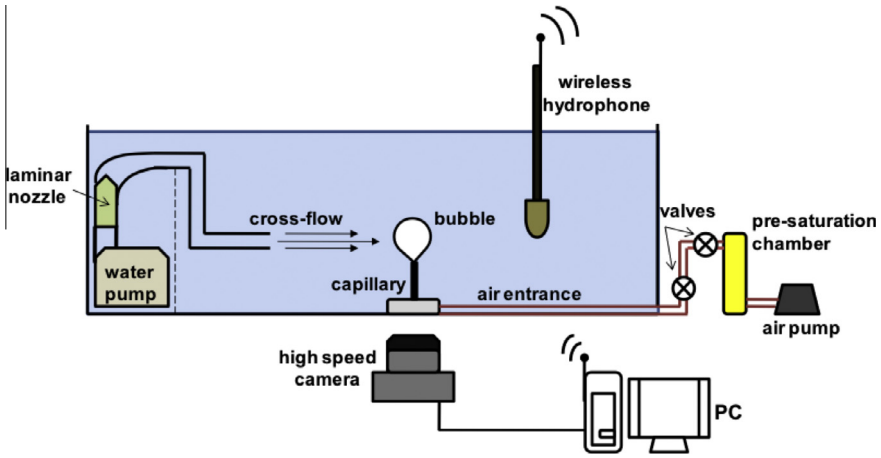

Fig. 1. Schematic of experimental set up.

Acoustic signals were recorded using a custom built, wireless piezoelectric hydrophone and were digitalized at 88.2 kHz and 16 bits [37]. The hydrophone probe was located an optimal distance of 5 cm from the capillary tube to minimize the perturbation to bubble behavior (formation and detachment), and to maximize the signal to noise ratio (SNR) of the acoustic signal as much as possible [35]. Finally video and acoustic data were synchronized and stored on a notebook PC.

3. Results

3.1. Bubble formation

In quiescent water, solitary bubbles with a final equivalent spherical radius of 1.33 mm (from video), form over a period of 32 ms (Fig. 2A). A time $t = 0$ ms, bubbles are initially spherical, although for $t = 32$ ms, they have a well-developed neck, which connects the capillary tube with the bubble, and the shape is a Cassini oval [37]. The bubble then separates from the glass tube and two lateral ripples travel across the bubble surface (36 ms). These ripples cause the bubble shape to approximate a spherical cap (36 ms and 40 ms), and then a trapezoidal form (46 ms). In this growth scenario, the lateral travelling ripples (from breaking the neck) generate y-axis symmetrical changes in the bubble edge (Fig. 2C) and then moderate the instantaneous bubble shape (Fig. 2A).

Bubble formation is quite different in the presence of a liquid cross-flow (Fig. 2B). Even for $t = 0$ ms, the bubble is not completely spherical, in this time-frame, the neck connects the capillary tube with the bubble body which is now less round and has a shape better described by a lemniscates [37]. The separation begins at 23 ms after the pinch off of the inclined air neck, and the bubble has a final equivalent spherical radius of 0.829 mm. Slightly after the bubble release ($t = 27$ ms), from the capillary tip, two lateral ripples are formed and travel away from the bubble's lower pole, traveling along the bubble surface. The ripples reach the bubble's upper pole at 33 ms; however, unlike quiescent conditions, the ripples now generate asymmetrical shape oscillations (Fig. 2D), with two vertical non-symmetric peaks seen in the bubble outline at $t = 33$ and 37 ms.

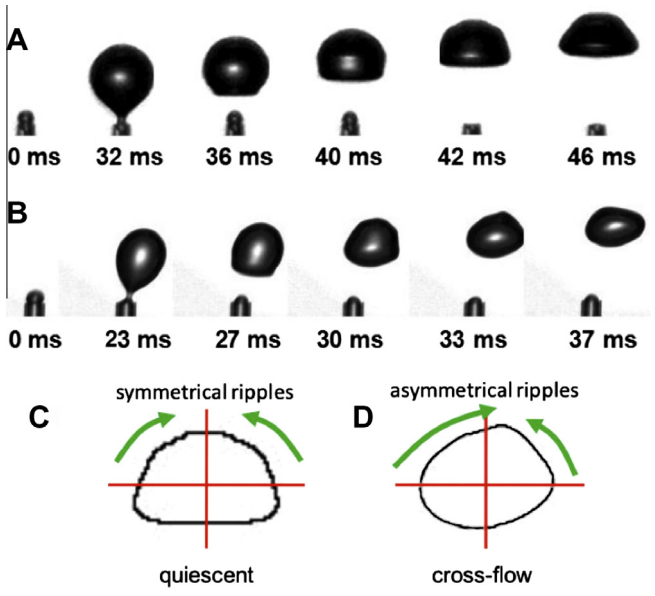

Fig. 2. Bubble video-photographs for quiescent (A) and cross-flow (B) respectively and the ripple observation in bubble edge (C and D).

3.2. Bubbles in the cross-flow

The acoustical responses for bubble formation in quiescent liquid and at different liquid flow rates (variables are v = cross flow velocity and Re = Reynolds number, where $Re = \rho v d/\mu$) were for the cross-flow are indicated in Fig. 3. Four liquid cross-flow cases tested: quiescent = 0 mm/s, weak = 30 mm/s, intermediate = 43 mm/s, strong = 128 mm/s. For comparison with the literature liquid flow speeds are non-dimensionalised with respect to bubble rise velocity for the quiescent case (77 mm/s). Thus the liquid cross-flow are now quiescent = 0, weak = 0.39, intermediate = 0.56 and strong = 1.66. For these cases, the bubble images for the moment before detachment are shown in Fig. 3a–d. The images show that with increasing cross-flow velocity the bubble-shape is distorted increasingly in the flow direction, producing non-symmetrical bubble formation (left flattening). In addition, depending on the drag-force imposed by the liquid, the bubble body develops an angle-inclination with respect to the vertical, which is in the 9–53° range. As a result, bubble size decreases with increasing v (Fig. 3d). For the train of acoustic pulses in the quiescent and weak flow tests (Fig. 3a and b), it is possible to observe clear (low noise) and constant amplitude pulses; in the contrary, for the intermediate and strong tests (Fig. 3c and d) an increment in noise increment and alternative amplitude changes are detected.

3.3. Fourier Spectral and Spectrogram analysis

For the quiescent case (Fig. 4I), the acoustical signal exhibits, for a time of order of 20 ms, a classical-freely-oscillating-lightly-damped acoustic signature, typical of bubble formation from a rigid glass capillary tube [24]. In this scheme, the bubble sound shows a high horizontal-axis oscillation-symmetry. Differences are apparent even for the weak case. Although the acoustical signal is similar to the $v = 0$ case, the sound duration is shortened (≈15 ms) and the horizontal oscillation-symmetry is maintained. For the intermediate cross flow case, the acoustic signal duration is shorter (≈10 ms), while horizontal oscillation-symmetry is lost, and a second wave-group becomes apparent. Finally, for the strong cross-flow case, the acoustic signature is even shorter (≈7 ms), horizontal oscillations are highly asymmetric and three wave-groups are evident.

Because these signals are rapidly changing and of short duration, Fourier Spectral Analysis (*FSA*) is used for a 4096 point, 29-pole and 128 point spectral approximation approach (MatLab Signal Processing Toolbox R2010b, MathWorks, U.S). The Hanning-Gaussian window was applied to acoustical data and two audio filters were applied; a low-pass filter (0.100–0.450 kHz) to eliminate noise attributable to the air pump, and a high-pass filter (2.2–3.0 kHz) to remove external noise caused by laboratory equipment (fluorescent lamp coil, motors, etc.). The results are shown in Fig. 4II for a time-series of 5 min. In the quiescent case, a single peak is predominant at 1.506 kHz corresponding to a Minnaert radius, R_0, of 1.99 mm, while for the weak flow case the dominant frequency has shifted to 1.649 kHz and has also broadened, which suggests a Minnaert radius of 1.82 mm. For the intermediate cross-flow, two frequency modes are observed in 1.758 kHz, 2.013 kHz and with a smaller amplitude; for this case, the predominant peak indicates a bubble radius $R_0 = 1.71$ mm. For the strong cross-flow, a range of acoustic peaks is detected (1.230, 1.688, 2.003, 2.531, 2.882 and 3.128 kHz), with the predominant being 2.882 kHz ($R_0 = 1.04$ mm). Spectral analysis shows that for increasing v, the dominant frequency increases, implying a smaller bubble formation, in agreement with video bubble size (Fig. 3a–d). The peak displacement is checked with the spectrogram methodology (2D frequency-time area) also for 5 min of recorded signal (Fig. 4III) which is applied again with a MatLab routine. The spectrogram

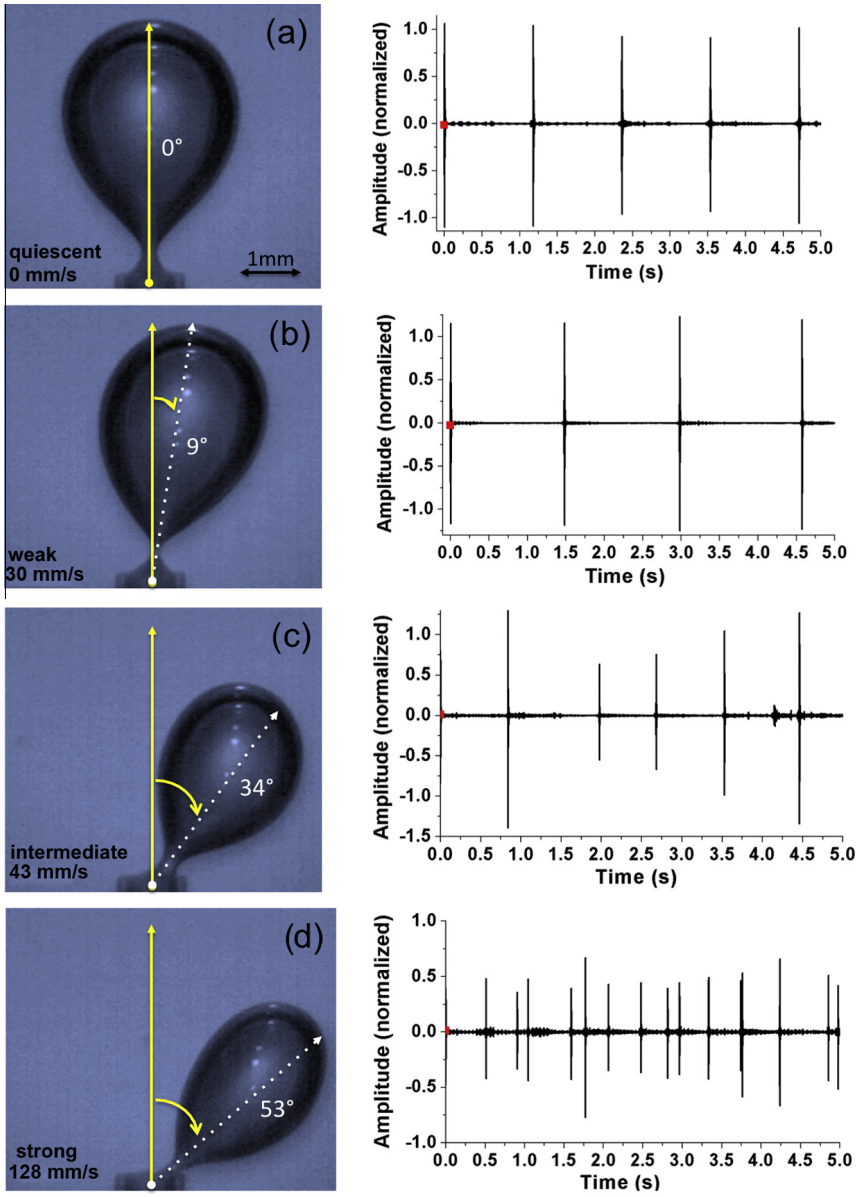

Fig. 3. Bubble photographs under a liquid cross-flow and acoustical pulses record by hydrophone.

results show color-spots located in regions that are in agreement with the predominant frequency-peaks observed with the *FSA* in Fig. 4II.

In order to facilitate the understanding of the results shown in Fig. 4, the predominant peaks for each case are normalized with respect to the Minnaert frequency (f_0) given in quiescent case (1.506 kHz) and are indicated in Fig. 5, in which it is possible observe when the liquid flow velocity increases, the predominant frequency (FFT) also to increases. This corroborates the results of Fig. 4.

4. Discussion

The acoustical signals (Fig. 4I) suggest that a possible explication of the pressure acoustical oscillations may be found in the beat pattern. The beat phenomenon are present when two oscillatory motions or waves have nearly the same frequency ($f_1 \approx f_2$), in contrast the amplitude (A) may be equal, although this is not necessary. A typically theoretical beat relation is:

$$\psi(t) = sin(2\pi f_1 t) + sin(2\pi f_2 t) = \left[2Acos\left(2\pi\frac{f_1 - f_2}{2}\right)t\right] sin\left(2\pi\frac{f_1 - f_2}{2}\right)t \quad (2)$$

While a typical, freely-oscillating, lightly-damped theoretical bubble sound emission is related to be of the form [26].

$$p(t) = Acos(f_b(t - t_0) + \varphi)exp\left(-\frac{f_b\delta(t - t_0)}{2}\right) \quad (3)$$

where $p(t)$ is the acoustic pressure, f_b is the bubble resonant frequency (when pinches off), δ is the damping factor, t_0 is the time at which the bubble takes off and φ is the phase factor.

Assuming two bubble sound signals (f_{b1}, f_{b2}) with the form indicated in Eq. (3) and performing a beat signal (Eq. (2)), the relation is [26].

$$p'(t) = A_1 cos[f_{b1}(t - t_0) + \varphi_1]exp\left[-\frac{f_{b1}\delta_1(t - t_0)}{2}\right] + A_2 cos[f_{b2}(t - t_0) + \varphi_2]exp\left[-\frac{f_{b2}\delta_2(t - t_0)}{2}\right] \quad (4)$$

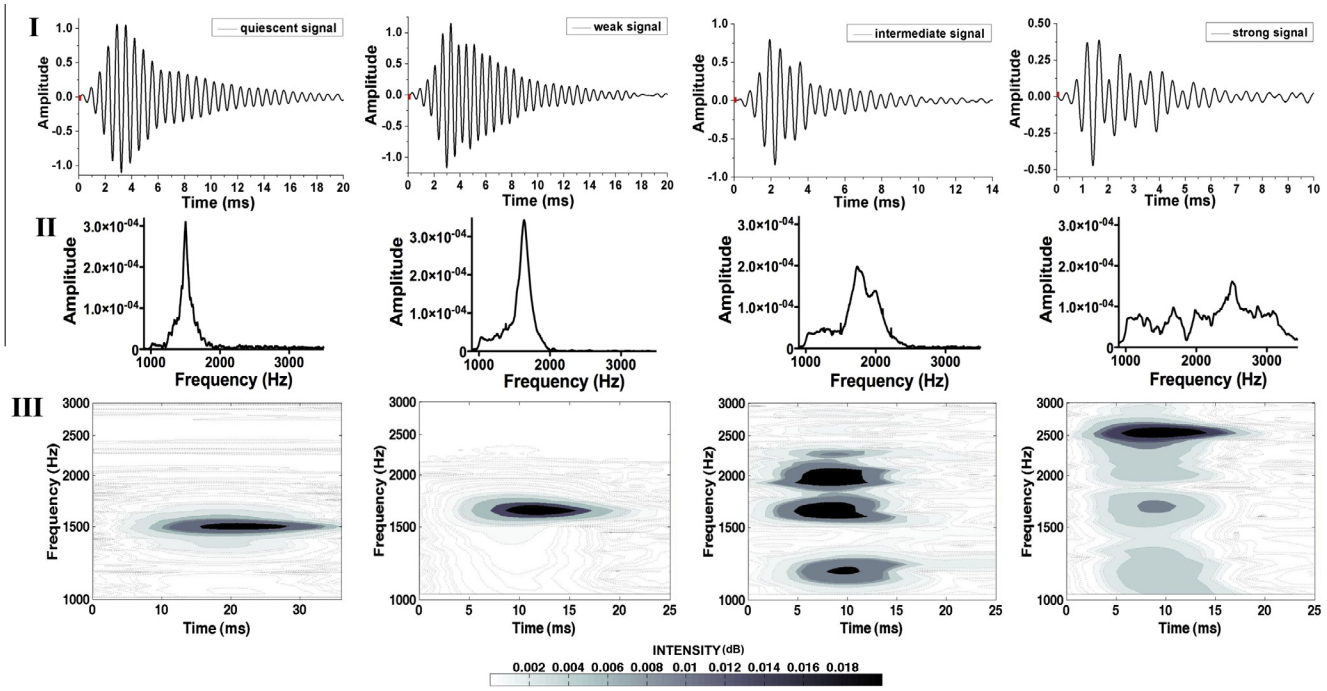

Fig. 4. (I) Acoustical signals for the cases to study and (II) Spectral, (III) Spectrogram analysis respectively.

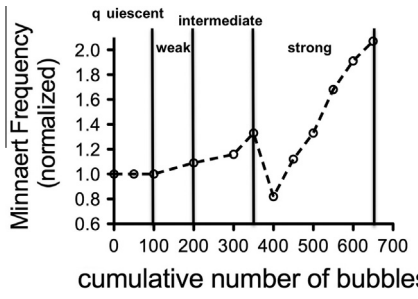

Fig. 5. Predominant peaks in the FFT normalized to Minnaert frequency.

Comparing the behavior of $p'(t)$ and the acoustical signals for intermediate and strong flows (Fig. 4I), it is possible to distinguish the appearance of one and two beats respectively. For the intermediate case, one beat is present near 4 ms after the time of maximum amplitude, while for strong cross-flow, beats are at 2.5 and 4 ms after the time of maximum amplitude. Experimental results by Deane and Stokes [26] show that a beat acoustical signal is the result of the bubble fragmentation in a fluid shear (the bubbles are produced 20 cm below of fragmentation zone). Certainly, two new bubbles are created in the fragmenting process and the acoustical signal detected by this event shows beat behavior, in other words, the beats are the acoustical signature in the fragmentation of a bubble with large volume. Deane and Stokes [26] explain the beat as the superposition of two acoustical signals of bubbles generated individually, in our case, surprisingly the beat is only detected when an intermediate-strong cross-flow is applied and we not have the birth of two new bubbles; in our case the possible source of the beat-signal is the asymmetric bubble growth. Deane and Stokes tested Eq. (4) for sound emission from a binary fragmentation event (bubbles fragmenting in a shear flow) through a combination of automated processing and human intervention. They found a close agreement between the measured emission and the theoretical model (specified by Eq. (4)). In our study, we used a Wolfram-Mathematica v.9 Nonlinear-Model-Fit routine package for obtain the fit (via Eq. (4)) to measure acoustical signal emission for the strong case (Fig. 4I). The frequencies for the waves in fit-adjustment are $f_{b1} = 2.882$, $f_{b2} = 2.531$ kHz which are taken from Fourier-Spectrogram analysis (Fig. 4II), and the other eight parameters are summarized in Table 1.

Each one of the theoretical oscillations (individually) and its superposition (in comparison with the experimental data) are plotted in Fig. 5. It is interesting to observe that oscillations in the f_{b1} and f_{b2} signals show different behavior; for f_{b1} the oscillations describe a light or underdamped system, while for f_{b2} an overdamped system is indicated. These two behaviors are superposed and compared with experimental-data (Fig. 6) showing a good agreement in frequency and an overestimation in the amplitude.

Certainly the beats signals are observed when the bubbles suffer a fragmentation process [26], but has also been detected in coalescence events [31] and when the bubbles are generated at the top of a bubble chain with a bubble formation rate of 8 Hz [28], which is well above our experimental value (0.33 Hz). Therefore in our study the appearance of beats by coalescence or bubble chain production is discounted. Strasberg [38] mentioned that changes of the shape in bubbles growing in an inclined capillary-glass tube (nonspherical) are associated with an increment and decrement of amplitude (an envelope) at low frequencies, very similar to beats, this it is in agreement with the results reported in this study and supports the possibility that beats can be originated by asymmetric bubble growth.

Finally in order to elucidate the mechanism responsible for the beat generation a synchronized sequence of acoustic and video data (images in binary-mode) for a solitary bubble is shown in Fig. 7. When the bubble it is connected to the capillary tube the

Table 1
Parameters calculated by computing algorithm.

Parameter / units	Wave 1	Wave 2
A / normalized	0.9	−0.79
f_b / rad s^{-1}	18,098	15,894
δ / dimensionless	0.078	0.03
t_0 / ms	0.00010	0.00018
φ / rad	−0.82	0.39

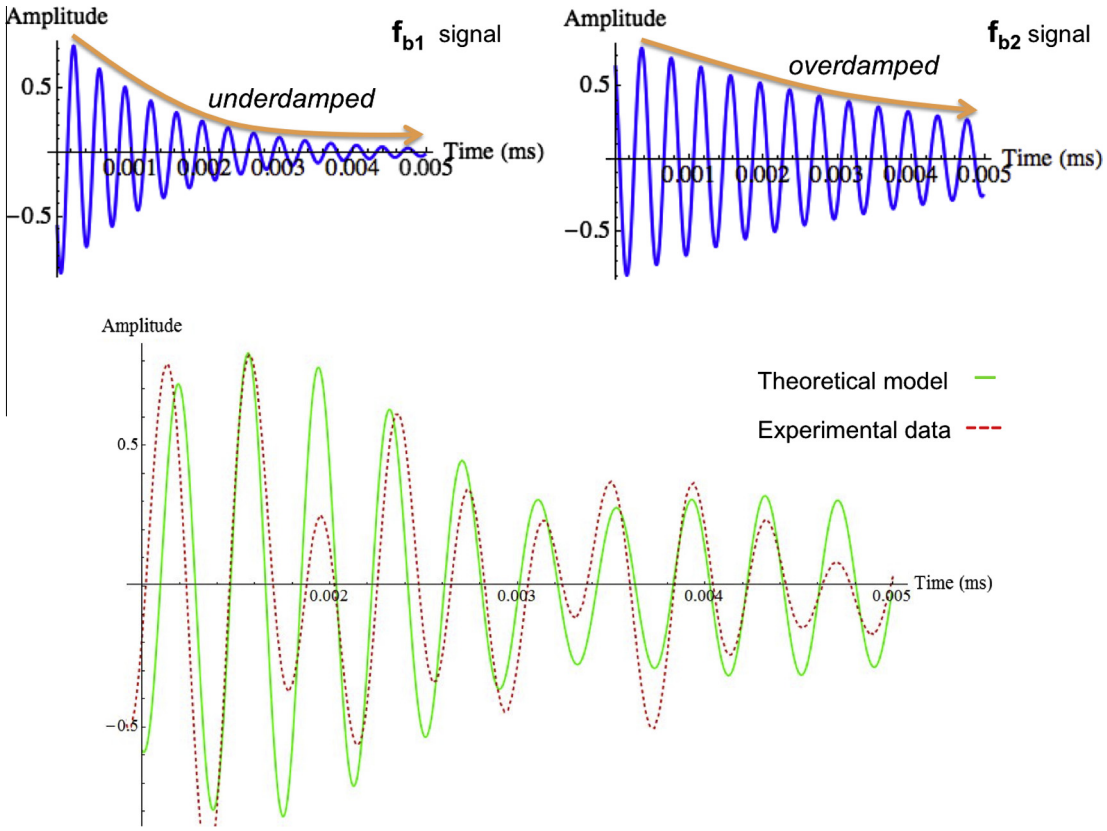

Fig. 6. Wave signals for the beat construction (above), and the comparison between the theoretical-model and the acoustical emission for the strong case (below).

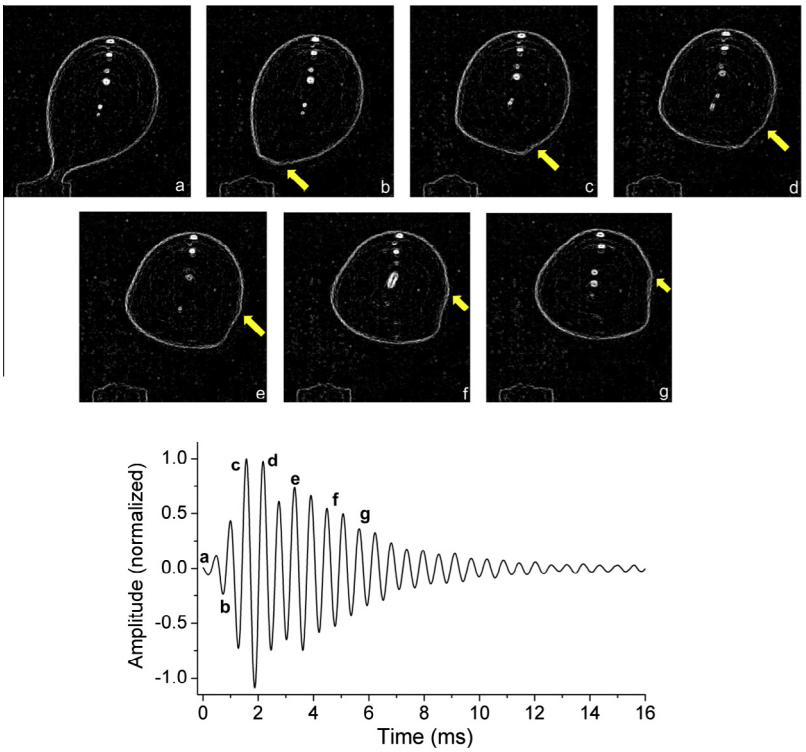

Fig. 7. Synchronous comparison between contour-shape bubble oscillations frames recorded at 1 ms (up) and the acoustic signal (below) for an intermediate flow regime.

acoustic pressure is zero and it is still possible to observe the bubble neck (a). In the moment that the air neck is broken, the amplitude of the acoustic signal decreases (fall in value), consistently with the volume forcing produced by the rapid change in the bubble shape just after pinch-off [27]. Then, the gas compressibility provokes bubble shape oscillations, which travel through the

entire surface from the bottom to the top of the bubble body as capillary waves, noted by changes in the bubble perimeter, (yellow-arrow in b-g). The previous oscillations travel on the bubble surface at a mean-speed of about 17.5 cm s^{-1} which gives rise to a frequency (imagining a longitudinal wave) of 87.5 Hz for a perturbation in the capillary wave regime (with a typical wavelength $\lambda \approx 2$ mm), which confirms that these oscillations or ripples are really capillary waves and they not are related to the frequencies of the passive acoustical signals for the intermediate flow rate of about 1.7–2.0 kHz produced when the bubble body detaches from the glass tube. The beat is produced when the bubble is in the position (e) and it can be compared with the bubble contour in the Fig. 2C. It is interesting to point out that the beat phenomena are not observed in the weak case (Fig. 3b-II), even when a cross flow is applied. The previous observations elucidate the existence of a critical liquid feed flow (v_{crit}) for that beat passive signal that can be observed by hydrophone, and this will motivated future studies.

5. Conclusions

Experiments on air bubbles generated at different liquid horizontal flow rates (quiescent, weak, intermediate and strong) are presented. In each case, high-speed photographs and acoustical responses are recorded for time series of 5 min. The photographic evidence indicates that horizontal flow affects the bubble formation: in quiescent water conditions, the bubble rises vertically, and when it separates from the glass tube, two-lateral ripples travel across the bubble surface (capillary waves) causing symmetric bubble shape oscillations, while a classical, freely-oscillating and lightly-damped acoustic signature is observed: on the other hand, when a liquid cross-flow is imposed, the bubble suffers a lateral inclination (in the flow direction) and at the separation point, the lateral ripples cause a non-symmetric bubble shape oscillations, thus the acoustic signature shows a beat phenomenon behavior (intermediate and strong cases).

It is also observed that, with increasing liquid cross-flow, the number of beats increases and the horizontal-symmetry of the signals is lost for the intermediate and strong cases. This is the result of bubble oscillations not being totally vertical after being subjected to an impulsive force (neck collapse) caused by the gas body inclination owing to the drag force imposed by the flow.

The strong flow case is fitted by a theoretical model indicating that beats are composed of two waves with under (f_{b1}) and over damped (f_{b2}) system-behavior respectively. In addition, the video-sound data comparison for liquid cross-flow indicates that the ripples are the result of tilted air-neck bubble collapse, and that the ripples or capillary waves exhibit a superposition phenomenon which may be considered as the explanation for the detection of the beat sound. Finally we believe that this basic experimental information is very useful for a future comparison with data for shallow marine field-data sediments and to obtain a better understanding of the methane bubble emissions.

Acknowledgements

The authors gratefully acknowledge to US MEXUS program for the financial support to make this study possible. In addition, the authors would like to express their gratefulness to Professor Patricia Goldstein & Ira Leifer for your comments, and also to an anonymous reviewer for their assistance in the proper use of the English language.

References

[1] W.V. Pinczewski, The formation and growth of bubbles at a submerged orifice, Chem. Eng. Sci. 36 (1981) 405–411.
[2] H. Tsuge, Hydrodynamics of bubble formation from submerged orifice, in: Cheremisinoff (Ed.), Encyclopedia of Fluid Mechanics, vol. 43, Gulf Publishing Corporation, Houston, TX, 1986, pp. 191–232.
[3] K. Teresaka, H. Tsuge, Bubble formation under constant-flow conditions, Chem. Eng. Sci. 48 (1993) 3417–3422.
[4] H. Oğuz, A. Prosperetti, Dynamics of bubble growth and detachment from a needle, J. Fluid Mech. 257 (1993) 11–145.
[5] D. Gerlach, G. Biswas, F. Durst, V. Kolobaric, Quasi-static bubble formation on submerged orifices, Int. J. Heat Mass Transf. 48 (2005) 425–438.
[6] A. Vazquez, I. Leifer, R.M. Sánchez, Consideration of the dynamic forces during bubble growth in a capillary tube, Chem. Eng. Sci. 65 (2010) 4046–4054.
[7] J.F. Clark, I. Leifer, L. Washburn, B.P. Luyendyk, Compositional changes in natural gas bubble plumes: observations from the coal oil point marine hydrocarbon seep field, Geo-Mar. Lett. 23 (2003) 187–193.
[8] I. Leifer, G.D. De Leeuw, G. Kunz, L. Cohen, Calibrating optical bubble size by the displaced mass method, Chem. Eng. Sci. 58 (23/24) (2003) 5211–5216.
[9] S.H. Marshall, Air bubble formation from an orifice with liquid cross-flow, PhD thesis, University of Sydney, Australia, 1990.
[10] G.M. Evans, C.D. Rielly, J.F. Davidson, K.J. Carpenter, Modelling and Design of a Gas-Inducing Reactor, American Institute of Chemical Engineers, Spring National Meeting, Houston, USA, 1991. Paper 33e.
[11] Y. Kawase, J.J. Ulbrecht, Formation of drops and bubbles in flowing liquids, Ind. Eng. Chem. Process Dev. 20 (1981) 636–640.
[12] S.H. Marshall, M.W. Chudacek, D.F. Bagster, A model for bubble formation from an orifice with liquid cross-flow, Chem. Eng. Sci. 48 (1993) 2049–2059.
[13] R.B.H. Tan, W.B. Chen, K.H. Tan, A non-spherical model for bubble formation with liquid cross-flow, Chem. Eng. Sci. 58 (2000) 287–295.
[14] R.B.H. Tan, W. Zhang, A model for bubble formation and weeping at a submerged orifice with liquid cross-flow, Chem. Eng. Sci. 55 (2003) 6259–6267.
[15] S. Ghaemi, P. Rahimi, D.S. Nobes, The effect of gas-injector location on bubble formation in liquid cross flow jets, Phys. Fluids 22 (2010) 043305.
[16] A.K. Ghosh, J.J. Ulbrecht, Bubble formation from a spargering polymer solutions-II. Moving liquid, Chem. Eng. Sci. 44 (1989) 969–977.
[17] A. Tomiyama, G.P. Celata, S. Hosokawa, S. Yoshida, Terminal velocity of single bubbles in surface tension force dominant regime, Int. J. Multiph. Flow 28 (2002) 1497–1519.
[18] K. Loubiere, G. Hebrard, Bubble formation from a flexible hole submerged in an inviscid liquid, Chem. Eng. Sci. 58 (2003) 135–148.
[19] K. Loubiere, G. Hebrard, Influence of liquid tension (surfactants) on bubble formation at rigid and flexible orifices, Chem. Eng. Process. 43 (2004) 1361–1369.
[20] I. Leifer, Characteristics and scaling of bubble plumes from marine hydrocarbon seepage in the Coal Oil Point seep field, J. Geophys. Res. 115 (2010) C11014.
[21] W.R.J. Boyd, J. Varley, The uses of passive measurement of acoustic emissions from chemical engineering processes, Chem. Eng. Sci. 56 (5) (2001) 1749–1767.
[22] W. Al-Masry, E. Ali, Y. Aqeel, Determination of bubble characteristics in bubble columns using statisticals analysis of acoustics sound measurements, Chem. Eng. Res. Des. 83 (2005) 1196–1207.
[23] A. Vazquez, R. Manasseh, R.M. Sánchez, G. Metcalfe, Experimental comparison between acoustic and pressure signals from a bubbling flow, Chem. Eng. Sci. 63 (2008) 5860–5869.
[24] M. Minnaert, On musical air-bubbles and sounds of running water, Phil. Mag. 16 (1993) 235–248.
[25] I. Leifer, D. Tang, The acoustic signature of marine seep bubbles, J. Acoust. Soc. Am. 121 (1) (2007) 35–40.
[26] G.B. Deane, M.D. Stokes, The acoustic signature of bubbles fragmenting in sheared flow, J. Acoust. Soc. Am. Exp. Lett. 120 (6) (2006) EL84–EL89.
[27] G.B. Deane, H. Czerski, A mechanism stimulating sound production from air bubbles released from a nozzle, J. Acoust. Soc. Am. 123 (2008) EL126–EL132.
[28] R. Manasseh, A. Nikolovska, A. Ooi, S. Yoshida, Anisotropy in the sound field generate by a bubble chain, J. Sound Vib. 278 (2004) 807–823.
[29] A. Ooi, A. Nikolovska, R. Manasseh, Analysis of time delay effects on a linear bubble chain system, J. Acoust. Soc. Am. 124 (2008) 815–826.
[30] A. Doinikov, R. Manasseh, A. Ooi, Time delays in coupled multibubble systems (L), J. Acoust. Soc. Am. 117 (2005) 47–50.
[31] R. Manasseh, G. Riboux, F. Risso, Sound generation on bubble coalescence following detachment, Int. J. Multiph. Flow 34 (2008) 938–949.
[32] T.G. Leighton, K.J. Fagan, J.E. Field, Acoustic and photographic studies of injected bubbles, Eur. J. Phys. 12 (1991) 77–85.
[33] C. Feuillade, Acoustically coupled gas bubbles in fluids: Time-domain phenomena, J. Acoust. Soc. Am. 109 (6) (2001) 2606–2615.
[34] D. Manley, Change of size of air bubbles in water containing a small dissolved air content, Br. J. Appl. Phys. 11 (1960) 38–42.
[35] R. Manasseh, R.F. LaFontaine, J. Davy, I. Shepherd, Y.G. Zhu, Passive acoustic bubble sizing in sparged systems, Exp. Fluids 30 (2001) 672–682.
[36] H. Tsuge, S. Hibino, Bubble formation from an orifice submerged in liquids, Chem. Eng. Commun. 22 (1983) 63–79.
[37] A. Vazquez, R.M. Sanchez, E. Salinas-Rodríguez, A. Soria, R. Manaseeh, A look at three measurement techniques for bubbles size determination, Exp. Therm. Fluid Sci. 30 (2005) 49–57.
[38] M. Strasberg, The pulsation frequency of nonspherical gas bubbles in liquids, J. Acoust. Soc. Am. 25 (3) (1953) 536–537.